QUANTUM INTERFERENCE OF CHARGED IDENTICAL PARTICLES

Raedt, Hans De; Michielsen, Kristel

Published in:
Annalen der Physik

DOI:
10.1002/andp.19955070706

Publication date:
1995

Ann. Physik 4 (1995) 679–695

Annalen
der Physik

Quantum interference of charged identical particles

Hans De Raedt and Kristel Michielsen

Institute for Theoretical Physics and Materials Science Centre, University of Groningen, Nijenborgh 4, NL-9747 AG Groningen, The Netherlands

Received 24 April 1995, revised version 14 June 1995, accepted 22 June 1995

Abstract. We present the results of a computer simulation study of charged-particle interferometry, combining features of both the Aharonov-Bohm and Hanbury Brown-Twiss experiment. In contrast to a previous theoretical analysis of this experiment, we find that the Aharonov-Bohm effect is also present in the cross-correlated two-particle intensity. A simple, time-independent scattering theory that leads to conclusions that are in concert with the simulation data is given.

Keywords: Quantum Interference; Identical Particles; Aharonov-Bohm Effect.

1 Introduction

A vast amount of interference phenomena can be understood in terms of interference of classical waves. In quantum mechanics a particle can interfere with itself [1], leading to interference effects which have no classical analog. Although photons and massive particles give rise to similar self-interference phenomena, it is of interest to investigate how the charge or the particle statistics modify the interference effects. In this paper we analyze a thought experiment, proposed by Silverman [2, 3], that addresses several important conceptual issues related to the interference of charged, identical quantum particles. This thought experiment is designed such that both the charge and statistics can have an effect on the interference. A first theoretical analysis of this thought experiment [2, 3], shows that effects of the charge of the particles are observable in the self-interference signal whereas they are absent in the correlated two-particle interference signal.

In this paper we demonstrate that this remarkable conclusion is not correct. We use a versatile computer simulation technique to perform the thought experiment for physically different situations. In the simulation of Silverman's thought experiment, effects of the charge of the particles show up in *both* the self-interference and the two-particle interference signal. The results we obtain are numerically exact and allow us to identify limitations of Silverman's analysis.

The remainder of the paper is organized as follows. In Section 2 we briefly review the Aharonov-Bohm (AB) effect and give an example of how it shows up in a computer simulation. The basic features of the Hanbury Brown-Twiss (HBT) experiment are discussed in Section 3, where we also introduce the minor modifications that are necessary to take the particle statistics into account. The combined AB-HBT thought experiment is analyzed in Section 4. We demonstrate that earlier theoretical work can-

not explain the computer simulation results and we also explain why this is so. Finally, in Section 5 we present a simple, Fraunhofer-like theory that is in qualitative agreement with the conclusion drawn from the computer simulation results. Technical details on the simulation technique that we use can be found in the Appendices A and B.

2 Aharonov-Bohm experiment

It is well known that in classical mechanics, the motion of a charged particle is not affected by the presence of electromagnetic fields in regions of space from which the particle is excluded. In classical physics the vector potential $\mathbf{A} = (A_x, A_y, A_z)$ and scalar potential are merely convenient mathematical tools from which the electric and magnetic fields may be calculated. In quantum physics the vector potential does acquire physical significance [4, 5]. According to Aharonov and Bohm [5], the presence of a vector potential itself can lead to measurable effects even though the particle never enters the region where the electromagnetic field is non-zero.

The existence of the AB effect and the interpretation of experiments designed to confirm its existence have been the subject of a long debate. A comprehensive review of the different viewpoints and experimental results is given in Ref. 6. Additional information can be found in Refs. 7, 8. Ingenious experiments [9, 10], theoretical work [11], and simulations [12] have given further support to the existence of the AB effect.

A schematic diagram of the AB thought experiment is depicted in Fig. 1. The source S sends charged particles towards the two-slit interferometer. Within the middle-block a local, but otherwise constant, magnetic field $\mathbf{B} = (0, 0, B(x,y))$ is present. Outside this block, $B(x,y) = 0$. In the AB thought experiment, the charged particle can only

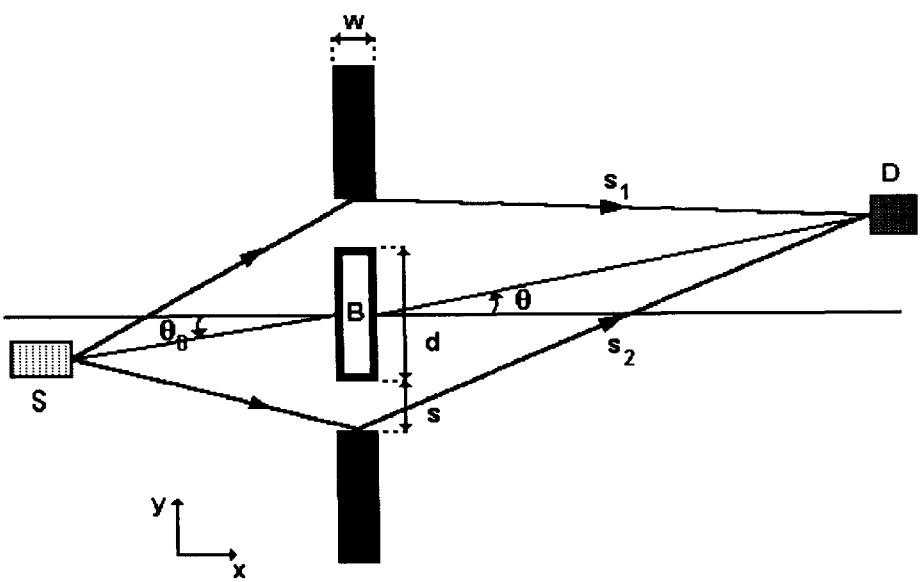

Fig. 1 Schematic diagram of the Aharonov-Bohm thought experiment. Particles leave the source S, pass through the double-slit and arrive at detector D. The particle does not experience the magnetic field B enclosed in the double-slit apparatus.

move in the field-free region of space. Therefore, in classical physics, the motion of a charged particle would never be affected by the presence of the magnetic field confined to the interior of the two-slit apparatus. However, for a charged quantum particle AB predict an observable phase shift in the interference pattern recorded at detector D, resulting from the presence of a non-zero vector potential in the region of space accessible to the particle. The phase shift itself depends on the flux enclosed by the two alternative paths s_1 and s_2.

The difference in the relative phase of paths s_1 and s_2 follows directly from the expression of the propagator $K(\mathbf{r},t;\mathbf{r}',t')$ for a particle to move from $\mathbf{r}'$ to $\mathbf{r}$ as a sum over paths [13, 14]

$$K(\mathbf{r},t;\mathbf{r}',t') = \sum_{\text{paths}} \exp\left\{\frac{i}{\hbar}\left(S_{\text{path}}^{(\mathbf{A}=0)}(\mathbf{r},t;\mathbf{r}',t') + e\int_{\text{path}} \mathbf{A}(\mathbf{r}'')\cdot d\mathbf{r}''\right)\right\} , \tag{2.1}$$

where $S_{\text{path}}^{(\mathbf{A}=0)}$ is the classical action along "path" with $\mathbf{A}=0$.

In our numerical work it is convenient to choose a gauge such that the vector potential takes the form

$$\mathbf{A} = (A_x(y),0,0) , \tag{2.2}$$

where $A_x(y) = -\int_0^y B(x,y')dy'$. In Appendix A it is shown that for a vector potential of this form, the motion of the particles is essentially in the (x,y)-plane. From Fig. 1 and (2.2) it is then clear that only particles that pass through the upper slit will experience a non-zero vector potential. Therefore, since $A_x = -Bd$ inside the upper slit, for paths of the type s_1, there will be an additional phase shift given by $\varphi = edwB/\hbar$. For particles taking route s_2 this phase shift is zero. Therefore the relative phase φ of the amplitudes for paths of type s_1 and s_2 is modified by an amount

$$\frac{\varphi}{\pi} = \frac{B}{B_0} , \tag{2.3}$$

where $B_0 = \pi\hbar/edw$ corresponds to a field that yields the maximum phase shift $\varphi = \pi$. For convenience we will express the magnetic field in units of B_0 in the following.

The intensity at the detector D is given by

$$P(D) = \left|\int_0^\infty dt \int d\mathbf{r}' K(\mathbf{D},t;\mathbf{r}',0)\psi_0(\mathbf{r}')\right|^2 , \tag{2.4}$$

where $\psi_0(\mathbf{r}')$ is the wave function describing the particles emitted by source S, and $\mathbf{D}$ is the position of the detector D.

Some computer simulation results [12] for the intensity on detector D are shown in Fig. 2 where the diffraction patterns for $B=0$ (solid line) and $B=B_0$ (dashed line) are superimposed. According to AB [5], maxima (minima) in the diffraction pattern for $B=B_0$ (or $\varphi=\pi$) should appear at the positions of the minima (maxima) in the diffraction pattern for $B=0$ and indeed, this (and all other) characteristic features of the AB effect are reproduced in the simulation [12]. We have also verified that the physical results do not depend on the choice of the gauge [12].

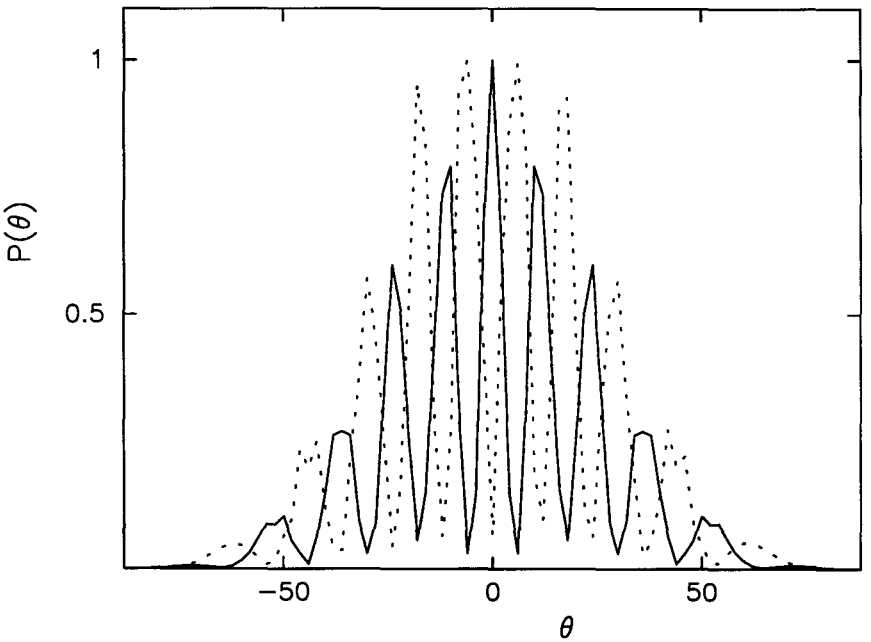

Fig. 2 Computer simulation results for the intensity on detector D (see Fig. 1). For this, and for all other simulation results presented in this paper, the dimensions of the double-slit are $s = \lambda_F$, $d = 4\lambda_F$ and $w = \lambda_F$, and the angle of incidence $\theta_0 = 0$. Solid line: $B = 0$, dashed line: $B = B_0$.

Assuming that the source S and detector D are both far away from the two slits, the qualitative features of the intensity $P(\theta)$ recorded by detector D are, to a good approximation, described by [12]

$$P(\theta) = \left\{\frac{\sin\left[2d\pi\left(\sin\theta - \sin\theta_0\right) + \varphi\right]}{\sin\left[d\pi\left(\sin\theta - \sin\theta_0\right) + \varphi\right]}\right\}^2 \left\{\frac{\sin\left(s\pi\sin\theta\right)}{s\pi\sin\theta}\right\}^2, \tag{2.5}$$

where the position of the source and detector are specified by θ_0 and θ respectively, s is the slit-size and d the distance between the slits (see Fig. 1). The result (2.5) shows that the interference pattern will shift by φ, a consequence of the presence of a magnetic field in a region of space from which the particles are excluded [5]. Note that the width w of the slit does not enter formula (2.5).

The conditions for the AB effect to be present can be summarized as follows: If there are at least two topologically different paths for the particle to travel from the source to the detector and if the integrals of the vector potential along these paths depend on the path taken, then the intensity pattern measured by detector D is a periodic function of the magnetic field B with period $2B_0$.

3 Hanbury Brown-Twiss experiment

A schematic representation of the Hanbury Brown-Twiss (HBT) experiment [15] is shown in Fig. 3. Thermal light emitted by the sources S_1 and S_2 is received by the

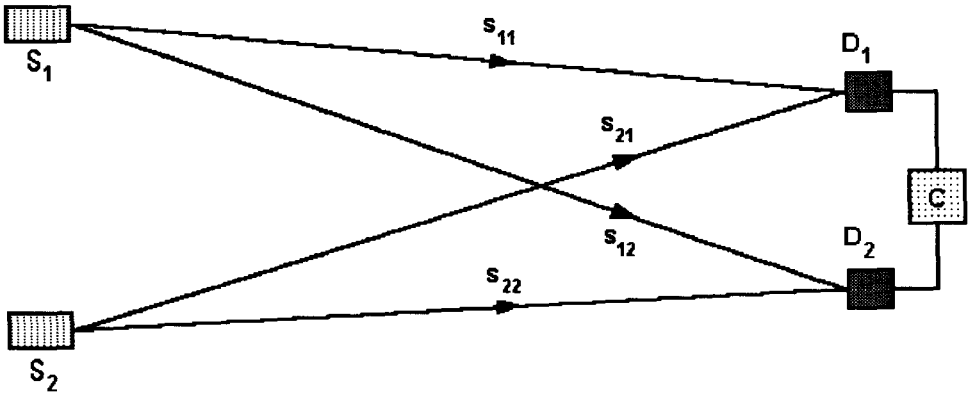

Fig. 3 Schematic representation of the Hanbury Brown-Twiss experiment. Particles leave the sources S_1 and S_2, and arrive at detectors D_1 and D_2. The signals of these detectors are multiplied in correlator C.

detectors D_1 and D_2. The signal produced at a detector is proportional to the intensity of the impinging light. The output of the detectors is multiplied together and the resulting electrical current is averaged over a substantial period of time. The experiments of HBT demonstrated that this cross-correlated signal exhibits an interference pattern as a function of the separation of the detectors. The results of the HBT experiment can be entirely understood in terms of classical wave theory. When extended to include quantum physics, the HBT experiment demonstrates that there are correlations in the arrival of photons that are emitted randomly from two different sources. This remarkable observation has been instrumental for the development of the theory of quantum optics.

Let us now explore the consequences of performing the HBT with massive quantum particles instead of with light. It is clear that if the particles are fermions, a description within the framework of classical wave theory is no longer adequate. For reasons that will become clear in section 4, we will treat the HBT thought experiment with fermions and bosons simultaneously.

The fermions or bosons emitted by the source S_1 generate signals at the detectors D_1 and D_2 as do the particles originating from the source S_2. The amplitude at detector D_m generated by the source S_n is given by

$$\psi_n(\mathbf{D}_m) = \int d\mathbf{k}\, g(\mathbf{k}) e^{i\mathbf{k}\cdot(S_n - D_m)} \; ; \quad m,n = 1,2 \; , \tag{3.1}$$

where $\mathbf{D}_m$ and S_n denote the position of the detector $\mathbf{D}_m$ and the source S_n respectively. For simplicity we assume that $g(\mathbf{k})$ is the same for both sources and is given by $g(\mathbf{k}) \propto \sigma \exp(-\sigma^2(\mathbf{k}-\mathbf{k}_F)^2/2)$, i.e. a Gaussian wave packet of width σ and mean $\mathbf{k}_F = (k_F,0,0)$. Here and in the following $k_F = 2\pi/\lambda_F$ whereby λ_F fixes the length scale.

The amplitude for the simultaneous arrival of one of the particles at detector D_1 and the other at detector D_2 is given by

$$\Psi(D_1,D_2) = \psi_1(D_1)\psi_2(D_2) \pm \psi_2(D_1)\psi_1(D_2) \; , \tag{3.2}$$

where the plus or minus sign reflects the fact that the particles are bosons or fermions respectively. The signal generated by the cross-correlator is

$$|\Psi(D_1, D_2)|^2 = \int d\mathbf{k} \int d\mathbf{k}' g(\mathbf{k})^2 g(\mathbf{k}')^2 (1 \pm \cos(\mathbf{k} - \mathbf{k}') \cdot (D_1 - D_2)) \ , \tag{3.3}$$

showing that there is an interference term depending on the relative distance between the two detectors. From (3.3) it follows that bosons are more likely to arrive in pairs ($\mathbf{D}_1 = \mathbf{D}_2$). For photons this effect, observed by HBT, is refered to as photon bunching. Fermions on the other hand avoid arriving in pairs, a direct consequence of the Pauli principle. Note that the interference term in (3.3) vanishes as $\sigma \to \infty$, i.e. when the waves emerging from the sources can be represented by a single plane wave.

4 AB-HBT thought experiment

The AB experiment provides information on the effect of the magnetic field on correlations of two *amplitudes*. The HBT experiment on the other hand yields direct information on the correlations of two *intensities*, i.e. of correlations of *four* amplitudes. Following Silverman [2, 3] we now consider a thought experiment that combines both the features of the AB and HBT set up and involves both the charge and the statistics of the particles.

A schematic view of this AB-HBT apparatus is shown in Fig. 4. Charged fermions (or bosons) are emitted by the source S and impinge on the double slit containing the confined magnetic field B. The particles passing through the slits generate signals at the de-

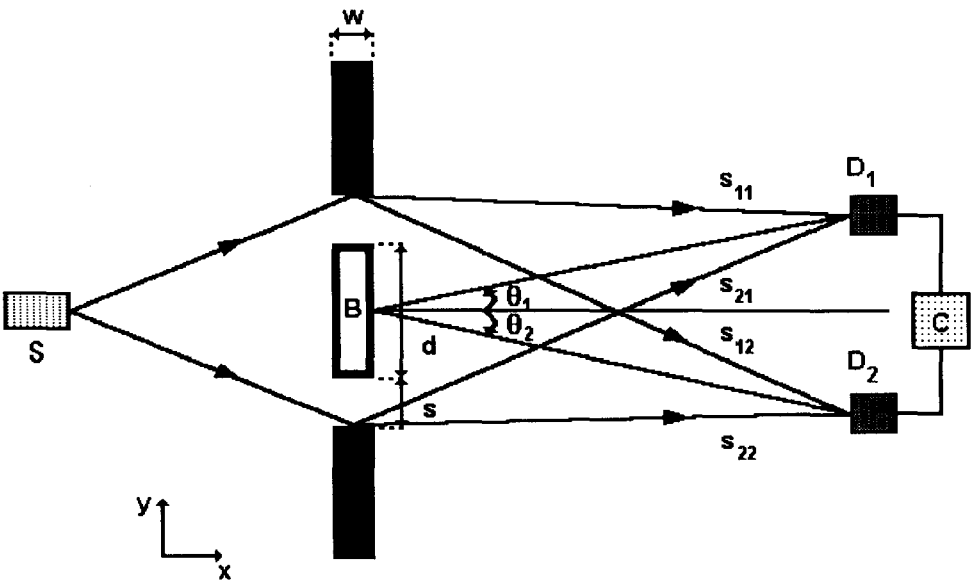

Fig. 4 Schematic view of the combined Aharonov-Bohm-Hanbury-Brown-Twiss apparatus. Particles leave the source S, pass through the double-slit and arrive at detectors D_1 and D_2. The signals of these detectors are multiplied in correlator C. The particles do not experience the magnetic field B enclosed in the double-slit apparatus.

tectors D_1 and D_2. In order for the particle statistics to be relevant at all, it is necessary that in the detection area the wave functions of two individual particles overlap.

The particle statistics may affect the single-particle as well as two-particle properties. The former can be studied by considering the signal of only one of the two detectors. Information on the latter is contained in the cross-correlation of the signals of both detectors.

Let us first reproduce Silverman's analysis [2, 3]. Assume that the double-slit apparatus can be designed such that the probability for two identical particles (fermions or bosons) to pass through the same slit can be made negligibly small. The two slits then act as the two sources in the HBT experiment with one modification: Due to the presence of the vector potential the waves can pick up an extra phase shift. For our choice of the vector potential (see (2.2)) only the wave emerging from the upper slit experiences a non-zero vector potential. The corresponding shift can be easily incorporated in the theory of the previous section by substituting

$$\mathbf{S}_1 \rightarrow \mathbf{S}_1 + (\varphi, 0, 0) \ , \tag{4.1}$$

where φ is given by (2.3).

Then, from (3.3) it immediately follows that the signal generated by the cross-correlator will *not* show any dependence on the confined magnetic field. According to Silverman [2, 3], the AB shifts for the direct process and the one in which the identical particles have been interchanged mutually cancel. Moreover, this cancelation is independent of the fact that the particles are fermions or bosons [16].

The basic assumption of Silverman's analysis is easily incorporated into a computer experiment. The initial two-particle wave function is a properly symmetrized product of single-particle wave functions, as shown schematically in Fig. 5a. The shaded circles indicate the extent to which the single-particle wave functions are non-zero (probability $>10^{-12}$). For simplicity the single-particle wave functions are taken to be Gaussians. Each Gaussian is positioned such that it effectively "hits" only one slit. A typical snapshot of the fermion probability is depicted in Fig. 5b. The upper (lower) part shows the fermion probability for $B = 0$ ($B = B_0$). The colored area in the middle block of the double slit (lower part) represents the confined magnetic field. The detectors (not shown) are placed very far at the right of the double slits. The intensity at the detectors is calculated using the procedure described in Appendix B.

From Fig. 5b it is clear that the fermion (and boson, not shown) probabilities for $B = 0$ and $B = B_0$ look identical. A more detailed analysis of the simulation results for the single (top) and correlated (bottom) detector signals for $B = 0$ for fermions (l.h.s.) as well as for bosons (r.h.s.) are presented in Fig. 6. For fermions the correlated signal for $\theta_1 = \theta_2$ vanishes, as required by the Pauli principle. Unfortunately this feature is hardly visible, due to the resolution we used to generate the pictures but it is present in the raw data. Within four digit accuracy, the corresponding data for $B = B_0$ (or, as a matter of fact, for any B) are identical to those for $B = 0$ and therefore they are not shown. Comparison of the cross-correlated intensities (bottom part) clearly lends support to Silverman's conclusion [2, 3]. However, it is also clear that the single-detector signals (upper part) do *not* exhibit the features characteristic of the AB effect. Under the conditions envisaged by Silverman, not only is there no AB effect in the cross-correlated signal: There is no AB effect at all.

The absence of the AB effect can be traced back to Silverman's assumption that the slits can be regarded as sources, thereby eliminating the second, topologically different,

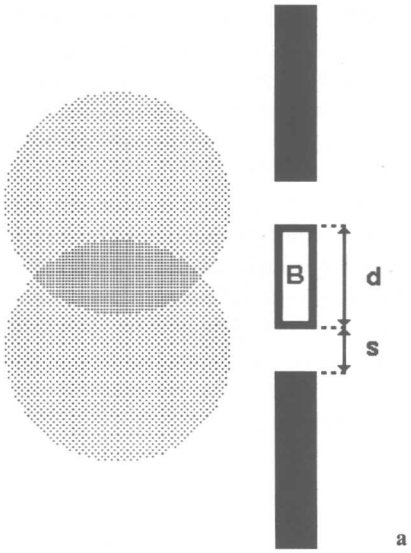

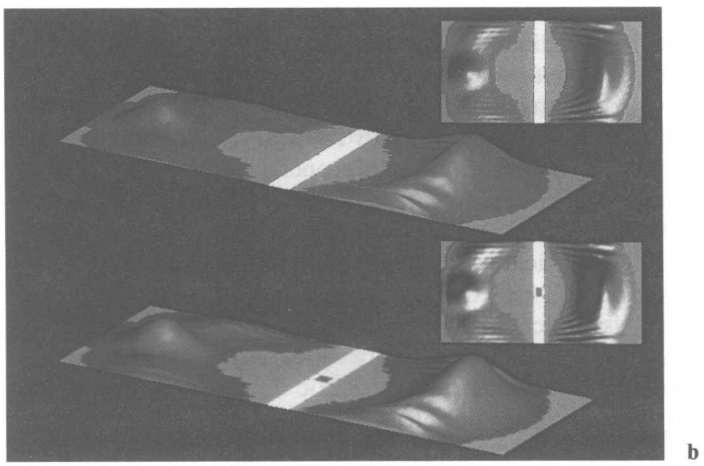

Fig. 5 **a.** Schematic diagram showing the extent of the initial single-particle wave functions from which the wave function for the fermion and bosons are build. Each wave packet is designed such that it effectively hits only one slit. **b.** Snapshot of the fermion probability distribution at time $t = 120\hbar/E_F$. The width of the initial Gaussian wave packets $\sigma = \lambda$. Upper part: $B = 0$, lower part: $B = B_0$.

alternative for a particle to reach the detector. A different route to arrive at the same conclusion is to invoke gauge invariance to choose the vector potential such that the two particles would never experience a non-zero vector potential.

A full treatment of the thought experiment depicted in Fig. 3 requires that *all* possibilities for *both* identical particles are included in the analysis. This is easily done in the computer experiment by changing the position and width of the Gaussians used to build the initial wave function of the fermions or bosons, as illustrated in Fig. 7a. In contrast to the previous case, schematically shown in Fig. 5a, the wave packets have

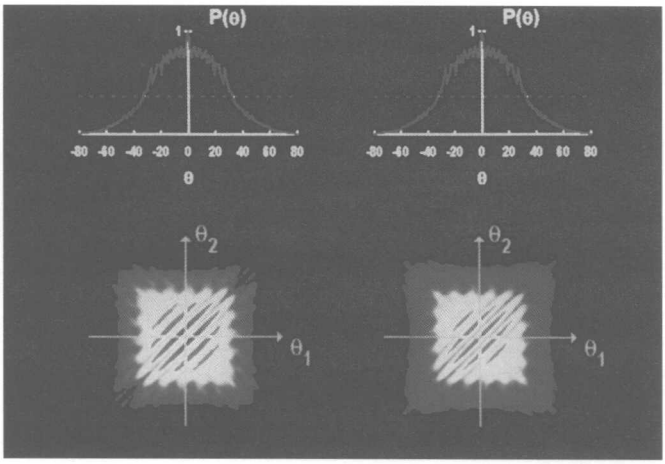

Fig. 6 Simulation results for single- (top) and correlated (bottom) detector signal for $B = 0$, obtained from the solution of the TDSE with the initial state sketched in Fig. 5a. On the left: Signals generated by fermions. On the right: Signals generated by bosons. The corresponding pictures for $B = B_0$ are identical and not shown.

been "designed" such that they both hit the two slits. A typical snapshot of the fermion wave function is depicted in Fig. 7b. The upper (lower) part shows the fermion probability for $B = 0$ ($B = B_0$). A close look at the upper and lower part shows that the positions of the maxima of the transmitted wave for $B = 0$ and $B = B_0$ are interchanged.

The results for the single (top) and correlated (bottom) detector signals for $B = 0$ and $B = B_0$ are shown in Figs. 8 and 9 respectively. Comparison of the upper parts of Figs. 8, 9 provides direct evidence of the presence of an AB effect. There is only a small quantitative difference between the fermion (l.h.s.) and boson (r.h.s.) signals: The interference fringes of the fermions are less pronounced than in the case of bosons, another manifestation of the Pauli principle.

The cross-correlated boson intensities (r.h.s. of the bottom part of Figs. 8, 9) clearly exhibit an AB-like effect. The positions of the maxima and minima are interchanged if the magnetic field changes from $B = 0$ to $B = B_0$. We have verified that the shift of these positions is a periodic function of the field B. These results for the case of boson statistics cannot be explained on the basis of Silverman's theory [2, 3].

The differences in the cross-correlated fermion intensities (l.h.s. of the bottom part of Figs. 8, 9) are not as clear as in the boson case. Subtracting the $B = 0$ from the $B = B_0$ signal and plotting the absolute value of this difference yields the patterns shown in Fig. 10. It is clear that also the cross-correlated fermion intensity exhibits features that are characteristic of the AB effect.

The high symmetry in all the correlated signals shown is due to our choice $B = B_0$. The fact that we recover this symmetry in our simulation data provides an extra check on our method. If B is not a multiple of B_0, this high symmetry is lost but the salient features of the signals remain the same.

Thus, from our numerical experiments, we conclude that in an AB-HBT experiment, an AB shift of the interference pattern will be observed in both the single and two-

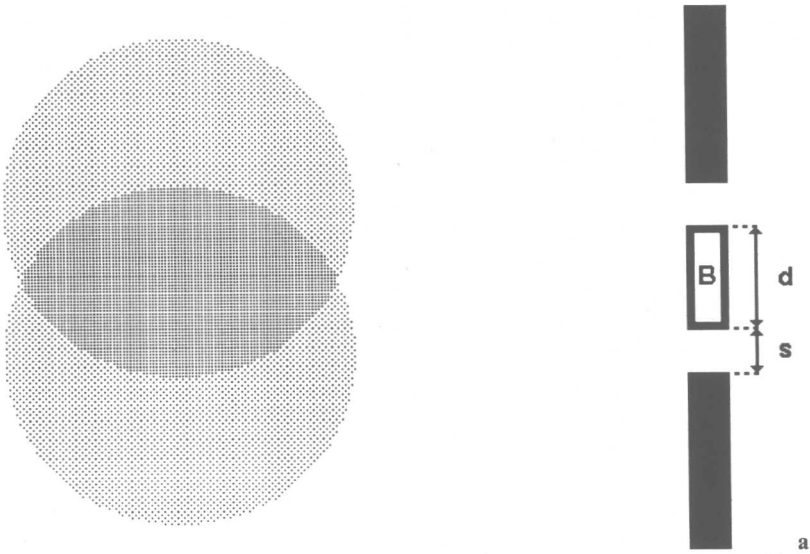

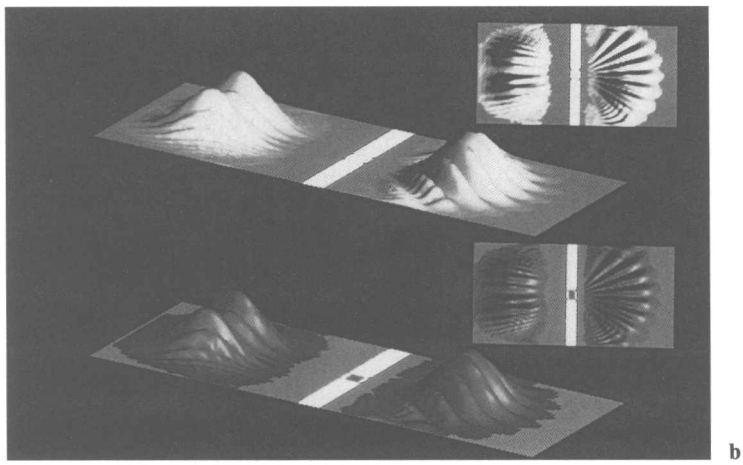

Fig. 7 **a.** Schematic diagram showing the extent of the initial single-particle wave functions from which the wave function for the fermion and bosons are build. Each wave packet is designed such that it effectively hits two slits. **b.** Snapshot of the fermion probability distribution at time $t = 168\hbar/E_F$. The width of the initial Gaussian wave packets $\sigma = 10\lambda$. Upper part: $B = 0$, lower part: $B = B_0$.

detector experiments. The AB effect (in both experiments) is more pronounced for bosons than for fermions.

5 Theory

Within the framework of Fraunhofer diffraction theory [17] it is straightforward to modify Silverman's analysis and account for all four interfering alternatives for each

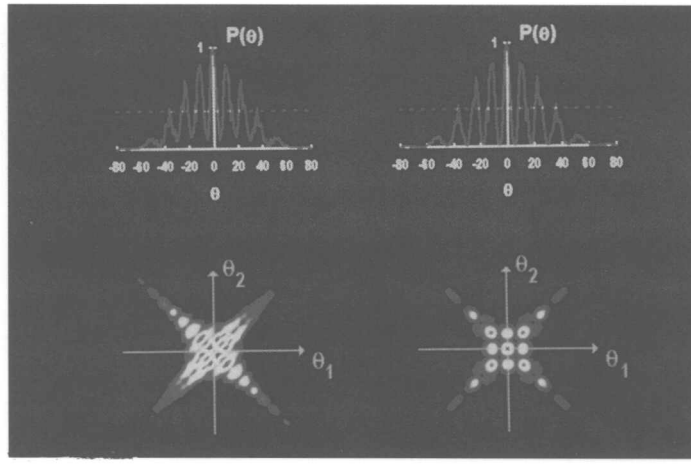

Fig. 8 Simulation results for single- (top) and correlated (bottom) detector signal for $B = 0$, obtained from the solution of the TDSE with the initial state sketched in Fig. 7a. On the left: Signals generated by fermions. On the right: Signals generated by bosons.

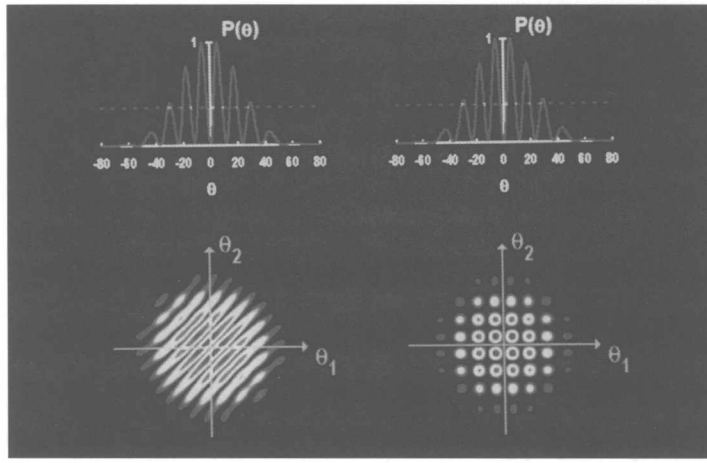

Fig. 9 Same as Fig. 8 except that $B = B_0$.

of the particles to travel from the source to the detector. There is no reason to expect that the results of such a theory will be in qualitative agreement with the numerical solution of the full problem [17]. However we will show that qualitatively, this simple theory is able to reproduce the salient features of the simulation results.

According to Fraunhofer diffraction theory, the amplitude at detector D_m resulting from a Gaussian wave packet impinging on the double slit from the left (see Fig. 4) is given by

$$\psi_n(\mathbf{D}_m) \propto \int d\mathbf{k}\, g(\mathbf{k})\, e^{i\mathbf{k}\cdot\mathbf{r}_n} \int_{\text{slit}} dy\, e^{i(k_F \sin\theta_m - k_y)y} \;; \quad m,n = 1,2 \;, \tag{5.1}$$

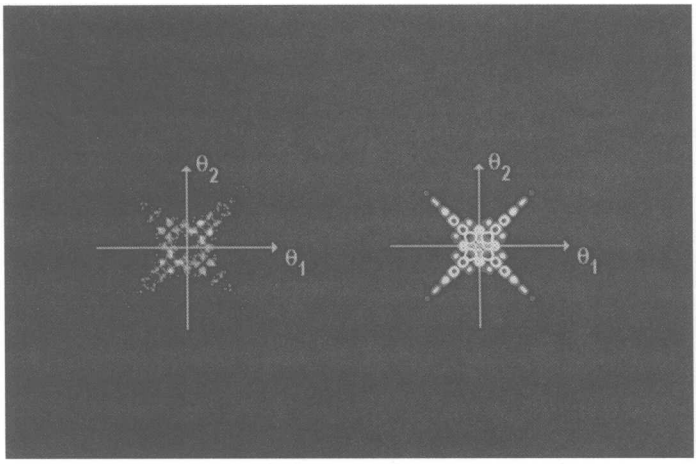

Fig. 10 Absolute value of the difference of the cross-correlated intensities of Figs. 8, 9.

where $\mathbf{r}_n$ denotes the center of the n-th wave packet at $t = 0$, and θ_m specifies the position of the detector m.

In the presence of the confined magnetic field, our choice (see (2.2)) of the vector potential will modify the phase of the wave emerging from the upper slit. Incorporating this phase shift into (5.1), using the fact that the problem is essentially two-dimensional, and performing the Gaussian integrals, the amplitude at detector m is easily shown to be

$$\psi_n(\mathbf{D}_m) \propto \int_0^S dy\, e^{-iyk_F \sin\theta_m} e^{-(y-y_n+d/2)^2/2\sigma^2} + e^{i(dk_F \sin\theta_m+\varphi)} \int_0^S dy\, e^{iyk_F \sin\theta_m} e^{-(y+y_n+d/2)^2/2\sigma^2} \quad ; \quad m,n = 1,2 \ . \tag{5.2}$$

The difference with Silverman's analysis is clear: Each of the two particles can contribute to the signal on one of the detectors by following two topologically different paths. Instead of four there are now sixteen interfering alternatives for the two particles to contribute to the cross-correlated signal.

From (5.2) and (3.2) it is clear that the overlap of the two initial wave functions will explicitly enter the expression of the signal on the cross correlator. In particular it is not difficult to see that for fermions, $||\psi_1 - \psi_2||$ and therefore also the cross-correlated signal vanishes with $|\mathbf{r}_1 - \mathbf{r}_2|$, assuming (as we did so far) that the Gaussian distribution for particle 1 and 2 is the same. In general, the cross-correlated signal will depend not only on the distance between the detectors, but on all the properties of the initial wave packets.

In comparison with the simulation technique employed to solve the full problem, it is a simple matter to combine (3.2) and (5.2) to calculate the single and correlated detector signals. Adopting the same model parameters as those used to obtain Figs. 8, 9 yields the results shown in Figs. 11, 12. Instead of the angular distribution for fermions or bosons, the upper part shows the single-particle angular distribution. For normal

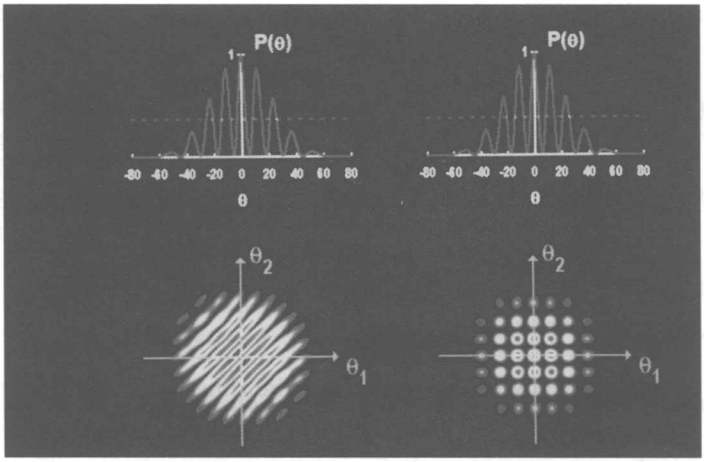

Fig. 11 Theoretical results for single- (top) and correlated (bottom) detector signal for $B = 0$, as obtained from Fraunhofer diffraction theory. Top part: Signal generated by a single particle. Bottom left: Signals generated by fermions. Bottom right: Signals generated by bosons.

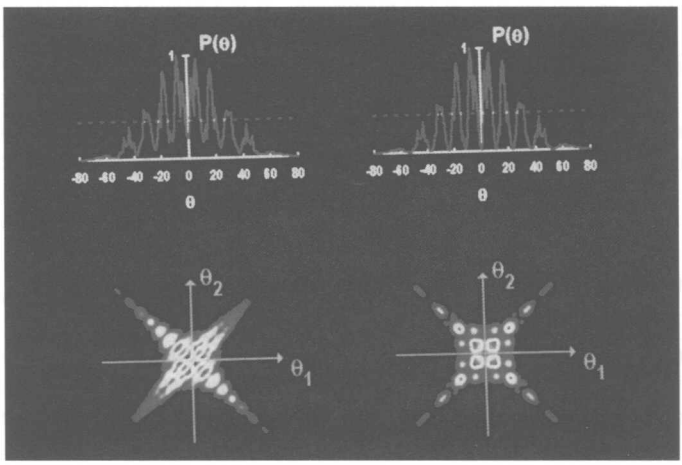

Fig. 12 Same as Fig. 11 except that $B = B_0$.

incidence (which is the case treated here) the agreement between the simulation and Fraunhofer results for the single-particle single-detector signal is excellent [12].

The main shortcoming of the simple Fraunhofer-based theory becomes evident by comparing the bottom part of, for instance, Figs. 8 and 11. Except for $\theta_1 \approx 0$ and $\theta_2 \approx 0$, diffraction effects are not treated properly, as is well-known [17]. However it is striking that this limitation of the Fraunhofer approach shows up much more clearly in the correlated two-particle signal than it does in the single particle signal.

Although (5.2) is only accurate if $\theta_1 \approx 0$ and $\theta_2 \approx 0$, it is nevertheless remarkable that the simple theory reproduces the salient features observed in the simulation. In particular, for the two-boson signal, there is good qualitative agreement (compare bot-

tom-right of Figs. 8, 11 and Figs. 9, 12 respectively). For the fermions, the agreement is not as good (compare bottom-left of Figs. 8, 11 and Figs. 9, 12 respectively). This is due to the fact that because of the Pauli principle, the cross-correlated signal may be large if $|\theta_1| \gg 0$, $|\theta_2| \gg 0$ and $\theta_1 \neq \theta_2$, and that is precisely the region where the Fraunhofer approach is expected to be less accurate. Taking all this into account, on a qualitative level the overall agreement between theory and numerical experiment is quite good and gives further support of the fact that the AB effect shows up in both the single and correlated detector arrangements, independent of the particle statistics.

6 Conclusions

The numerically exact solution of the time-dependent Schrödinger equation and the solution of the time-independent scattering problem for the combined Aharonov-Bohm-Hanbury-Brown-Twiss apparatus demonstrate that both the single-particle and correlated two-particle detector signals simultaneously exhibit features characteristic of the Aharonov-Bohm effect. These effects are more pronounced for bosons than they are for fermions.

We are grateful to M. Silverman for extensive and stimulating correspondence and discussions and for a critical reading of the manuscript. It is a pleasure to thank N. García for helpful suggestions. This work is part of a research programme of the "Stichting voor Fundamenteel Onderzoek der Materie (FOM)", which is financially supported by the "Nederlandse Organisatie voor Wetenschappelijk Onderzoek (NWO)". Computer simulations were carried out in the context of a project of the "Stichting Nationale Computer Faciliteiten (NCF)". This work is partially supported by an EEC Human Capital and Mobility project.

Appendix A: Computer simulation technique

The Hamiltonian for a system of two identical charged but non-interacting particles in an external, static magnetic field reads

$$\mathscr{H} = \mathscr{H}_1 + \mathscr{H}_2 \ , \tag{A.1a}$$

where

$$\mathscr{H}_n = \frac{1}{2m}(\mathbf{p}_n - e\mathbf{A}(\mathbf{r}_n))^2 + V(\mathbf{r}_n) \ ; \quad n = 1,2 \ , \tag{A.1b}$$

and m is the mass of the particle with charge e, $\mathbf{p}_n = -i\hbar\nabla_n$ is the momentum operator of particle n, and $\mathbf{A}$ represents the vector potential. The potential $V = V(x,y)$ will be used to specify the geometry of the apparatus. For numerical work, there is no compelling reason to adopt the Coulomb gauge (div $\mathbf{A} = 0$). A convenient choice for the vector potential is $\mathbf{A} = (A_x(x,y),0,0)$ where

$$A_x(x,y) = -\int_0^y B(x,y)\,dy \ . \tag{A.2}$$

Then the problem is essentially two-dimensional and the motion of the particles may be confined to the $x-y$ plane.

The simulation approach employed in this paper consists of numerically solving the time-dependent Schrödinger equation (TDSE)

$$i\hbar \frac{\partial}{\partial t} |\Phi(t)\rangle = \mathscr{H} |\Phi(t)\rangle \ , \tag{A.3}$$

where $|\Phi(t)\rangle$ represents the state of the system described by the Hamiltonian $\mathscr{H}$. The formal solution of the TDSE is given by

$$|\Phi(m\tau)\rangle = e^{-im\tau\mathscr{H}} |\Phi(t=0)\rangle \ , \tag{A.4a}$$

$$= e^{-im\tau\mathscr{H}_1} e^{-im\tau\mathscr{H}_2} |\Phi(t=0)\rangle \ , \tag{A.4b}$$

where $m = 0, 1, \ldots$ counts the number of time-steps τ and use has been made of the fact that the particles do not interact.

The initial state $|\Phi(t=0)\rangle$ can be written as a properly symmetrized product of single-particle wave functions

$$\langle \mathbf{r}_1, \mathbf{r}_2 | \Phi(0)\rangle = \phi_1(\mathbf{r}_1)\phi_2(\mathbf{r}_2) \pm \phi_2(\mathbf{r}_1)\phi_1(\mathbf{r}_2) \ . \tag{A.5}$$

A convenient choice for $\phi_n(\mathbf{r})$ is

$$\phi_n(x,y) \propto e^{2\pi i k_F (x\cos\theta_n + y\sin\theta_n)} e^{-(x-x_n)^2/2\sigma^2} e^{-(y-y_n)^2/2\sigma^2} \ , \tag{A.6}$$

i.e. a Gaussian wave packet centered around (x_n, y_n) with energy $\langle \phi_n | \mathscr{H} | \phi_n \rangle = E_F$ and width σ. In free space, the wave packet (A.6) moves in the $(\cos\theta_n, \sin\theta_n)$-direction. In practice the initial wave packet is normalized such that $\int |\Phi(x,y,t=0)|^2 dx dy = 1$.

From the formal solution (A.4) of the TDSE it follows that

$$\langle \mathbf{r}_1, \mathbf{r}_2 | \Phi(t)\rangle = \phi_1(\mathbf{r}_1, t)\phi_2(\mathbf{r}_2, t) \pm \phi_2(\mathbf{r}_1, t)\phi_1(\mathbf{r}_2, t) \ , \tag{A.7}$$

showing that the time-dependent wave function of the two-particle system can be constructed from the time-dependent wave functions of the individual single-particle systems. This is a major simplification because we can now solve the two-particle problem by solving two *independent* one-particle problems.

A detailed description of the method we use to solve the one-particle TDSE is given elsewhere [12]. The algorithm is based on a product formula introduced by Suzuki [18]. Important advantages of the TDSE approach are its reliability and flexibility. The former stems from the mathematical framework underlying the algorithm: The method is numerically stable and convergent under all circumstances. The latter derives from the fact that it can handle arbitrary geometries and (vector) potentials, providing a unified framework to investigate various physical problems.

In practice we solve the TDSE subject to the boundary condition that the wave function is zero outside the simulation box, i.e. we assume perfectly reflecting boundaries. The implementation we use is accurate to fourth-order in both the spatial and temporal mesh size, efficient and runs very efficiently on scalar, vector and parallel computer architectures [12]. Additional technical details can be found elsewhere [12].

For computational purposes we express distances in units of length λ_F, wavevectors are measured in units of $k_F = 2\pi/\lambda_F$, energies in $E_F = \hbar^2 k_F^2/2m$, time in $\hbar/E_F$ and

vector potential in units of $e\lambda_F/\hbar$ such that all physical quantities become dimensionless.

Appendix B: Data analysis

The final step is to analyze the wave packet transmitted by the two-slit arrangement. For the present purposes, it is not of great interest to compute the diffraction pattern on a screen placed near to the interferometer. Instead it is more appropriate to calculate the interference fringes on a screen at infinity. This can be done in the following way [19]. After the scattering event has taken place, the transmitted (and also the reflect) wave packet moves in free space (for a vector potential of the form (2.2)). Then the angular distribution of the intensity $P(\theta)$ on the screen at infinity can be written in terms of the Fourier transform of the transmitted wave packet [19]. For the case at hand the normalized $P(\theta)$ is given by

$$P(\theta) = \frac{\int_0^\infty |\tilde{\Phi}(q_x, q_y = q_x \tan\theta, t = T)|^2 dq_x}{\max_\theta \int_0^\infty |\tilde{\Phi}(q_x, q_y = q_x \tan\theta, t = T)|^2 dq_x} , \tag{B.1}$$

where $|\tilde{\Phi}\rangle$ is the Fourier transform of $|\Phi\rangle$ with respect to the spatial coordinates and T is the time required to complete the scattering event.

The expression of the normalized cross-correlated intensity $P(\theta_1, \theta_2)$ is obtained in a manner completely analogous to the one used to derive (B.1). Starting from the expression for the amplitude at $\mathbf{r}_1$ and $\mathbf{r}_2$ and at time t

$$\Phi(\mathbf{r}_1, \mathbf{r}_2, t) = \phi_1(\mathbf{r}_1, t)\phi_2(\mathbf{r}_2, t) \pm \phi_2(\mathbf{r}_1, t)\phi_1(\mathbf{r}_2, t) , \tag{B.2}$$

and using the fact that for $t \geq T$ the wave moving towards the detectors propagates freely, we obtain

$$P(\theta_1, \theta_2) = \frac{\int_0^\infty q_x^2 |\tilde{\Phi}(q_x, q_y = q_x \tan\theta_1, t = T)\tilde{\Phi}(q_x, q_y = q_x \tan\theta_2, t = T)|^2 dq_x}{\max_{\theta_1, \theta_2} \int_0^\infty q_x^2 |\tilde{\Phi}(q_x, q_y = q_x \tan\theta_1, t = T)\tilde{\Phi}(q_x, q_y = q_x \tan\theta_2, t = T)|^2 dq_x} . \tag{B.3}$$

The presence of the extra factor q_x^2 in the two integrals in (B.3) reflects the fact that we carry out an equal-time coincidence measurement.

References

[1] P.M. Dirac, The Principles of Quantum Mechanics. Oxford, London 1958
[2] M.P. Silverman, Am. J. Phys. **61**, 514 (1993)
[3] M.P. Silverman, And Yet It Moves: Strange Systems and Subtle Questions in Physics. Cambridge, New York 1993
[4] W. Ehrenberg, R.E. Siday, Proc. Phys. Soc. London **B 62**, 8 (1949)
[5] Y. Aharonov, D. Bohm, Phys. Rev. **115**, 485 (1959)
[6] M. Peshkin, A. Tonomura, The Aharonov-Bohm Effect. Springer, Berlin, 1989
[7] S. Olariu, I. Popescu, Rev. Mod. Phys. **57**, 339 (1985)
[8] A. Tonomura, Adv. Phys. **41**, 59 (1992)

[9] A. Tonomura et al., Phys. Rev. Lett. **48**, 1443 (1982)
[10] G. Badurek et al., Phys. Rev. Lett. **71**, 307 (1993)
[11] M. Jursa, P. Kasperkovitz, Phys. Rev. **A 47**, 3602 (1993)
[12] H. De Raedt, K. Michielsen, Computers in Physics **8**, 600 (1994)
[13] R.P. Feynman, A.R. Hibbs, Quantum Mechanics and Path Integrals. McGraw-Hill, New York 1965
[14] G. Baym, Lectures on Quantum Mechanics. Benjamin, London 1974
[15] R. Hanbury-Brown, R.Q. Twiss, Nature **177**, 27 (1956)
[16] M.P. Silverman, private communication
[17] M. Born, E. Wolf, Principles of Optics. Pergamon, New York 1959
[18] M. Suzuki, J. Math. Phys. **32**, 400 (1991)
[19] K. Michielsen, H. De Raedt, J. Phys.: Condens. Matter **3**, 8247 (1991)